JACS
JOURNAL OF THE AMERICAN CHEMICAL SOCIETY
Article
pubs.acs.org/JACS

Joining of Multiple Duplex Stems at a Single Quadruplex Loop

Kah Wai Lim,[†] Thi Quynh Ngoc Nguyen,[†] and Anh Tuân Phan*

School of Physical and Mathematical Sciences, Nanyang Technological University, 637371 Singapore

Supporting Information

ABSTRACT: We report here the formation of stable DNA quadruplex–duplex hybrid complexes harboring multiple duplex stems within the same loop of a quadruplex structure. The folding topology of a two-stem quadruplex–duplex hybrid construct was validated using nuclear magnetic resonance (NMR) spectroscopy. This multi-stem incorporation principle is applicable at different loop positions of the same quadruplex construct and could be extended to three or more duplex stems, giving rise to a diverse range of possible structures. These multi-stem complexes offer new design principles for the assembly of DNA architectures. The potential existence of such complex motifs in genomic sequences could have biological implications and would represent novel targets for drug development.

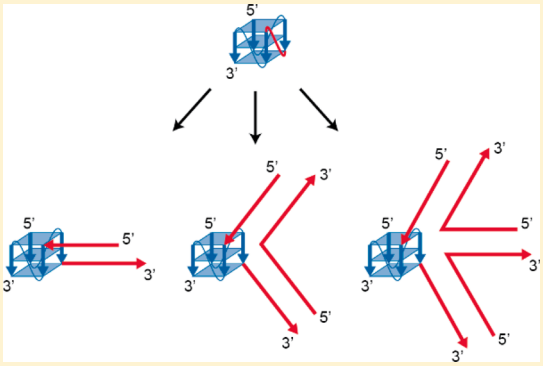

INTRODUCTION

A nucleic acid junction arises with the confluence of two or more distinct helical segments. Branched nucleic acid junctions[1] such as three- and four-way junctions have been implicated in DNA recombination[2] and repair,[3] and they could also serve as RNA architectural elements.[4] Variants of the four-way junction, which preferentially adopts a robust stacked X arrangement under certain environments,[5] are widely utilized in the construction of DNA nanomaterials.[6] On the other hand, a nucleic acid junction can also mediate the transition between two separate helical domains, as in the case of the DNA B–Z junction.[7]

A quadruplex–duplex junction[8] is formed upon the connection of a duplex helix onto a G-quadruplex, a four-stranded helical structure[9,10] made up of multiple G·G·G·G tetrads.[11] The connectivity between a single duplex and a quadruplex has been established across the various edges of a quadruplex core, in both coaxial and orthogonal manners,[8] illustrating the facile juxtaposition of these two structural elements. These quadruplex–duplex hybrid complexes have been shown to display high mechanical[12] and thermal stability[13] and diverse functionalities.[14−16] In addition, multiple duplex stems can be coordinated onto a single quadruplex scaffold through their separate connection at distinct edges of the tetrad core.[8] These observations point to the feasibility of the tetrad core serving as an organizational platform on which diverse nucleic acid structural elements can be coordinated.

Previous genome-wide analysis of quadruplex-forming motifs yielded over 350 000 hits across the human genome.[17,18] These studies have revealed a strong penchant for G-quadruplex formation within certain biologically important loci,[19] including oncogenic promoters,[20] introns,[21] and untranslated regions of mRNA.[22] Thermodynamic studies on quadruplexes have generally concluded that a long, disordered loop dramatically reduces the stability of a quadruplex.[23−25] In the event that a structured loop can be established, e.g., a duplex stem-loop for quadruplex–duplex hybrids, the destabilizing effect of a long loop would no longer apply; the structured loop could instead increase the robustness of the overall structure.[13] The possibility of formation of such stable quadruplex–duplex hybrid structures would further expand the sequence space of quadruplex-forming motifs.

Here, we demonstrated the simultaneous incorporation of two and three duplex stems within a single loop of a quadruplex. We further showed that such multi-stem incorporation approach is applicable at different loop positions of the same quadruplex construct, giving rise to a diverse range of possible structures.

RESULTS AND DISCUSSION

Two-Stem Quadruplex–Duplex Hybrid Construct *2S-QDHL2*. Starting from an all-parallel-stranded G-quadruplex scaffold,[26,27] two duplex stems were incorporated across a single propeller loop of the G-tetrad core (Figure 1a). One-dimensional imino proton NMR spectrum of this two-stem construct, d[TT **GGG** T **GGG** T (CGCGAA GCA TTCGCG) (ATCTGA GAA TCAGAT) T **GGG** T **GGG** T] (G-tracts are in bold; individual duplex stems are enclosed by parentheses, in which two complementary tracts are underlined) (henceforth denoted *2S-QDHL2*; Table 1), supported the formation of a single predominant quadruplex–duplex hybrid structure (Figure 2a). Twelve major sharp peaks at ∼11–12 ppm (Figure 2a, labeled with filled circles) indicated the formation of a three-layered G-tetrad core, whereas at least nine peaks at ∼12.6–14 ppm indicated the formation of Watson–Crick base pairs of the two duplex stems. Chemical shift patterns of the

Received: August 1, 2014
Published: December 2, 2014

   dx.doi.org/10.1021/ja5078816 | J. Am. Chem. Soc. 2014, 136, 17969–17973

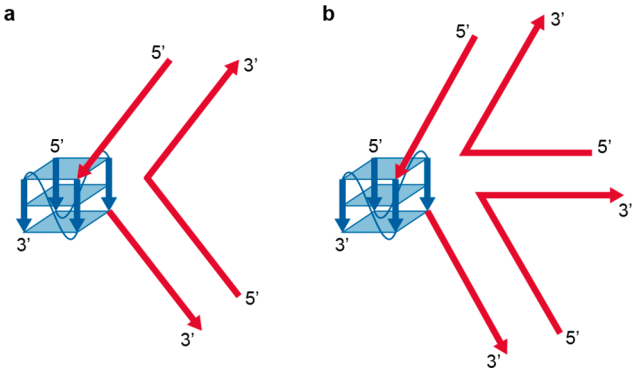

Figure 1. Joining of multiple duplex stems at a single loop of a G-quadruplex scaffold. Attachment of (a) two and (b) three duplex stems onto the middle propeller loop of an all-parallel-stranded G-tetrad core. G-tracts are colored in blue, while duplex stems are colored in red. G-tetrad layers are represented as blue planes.

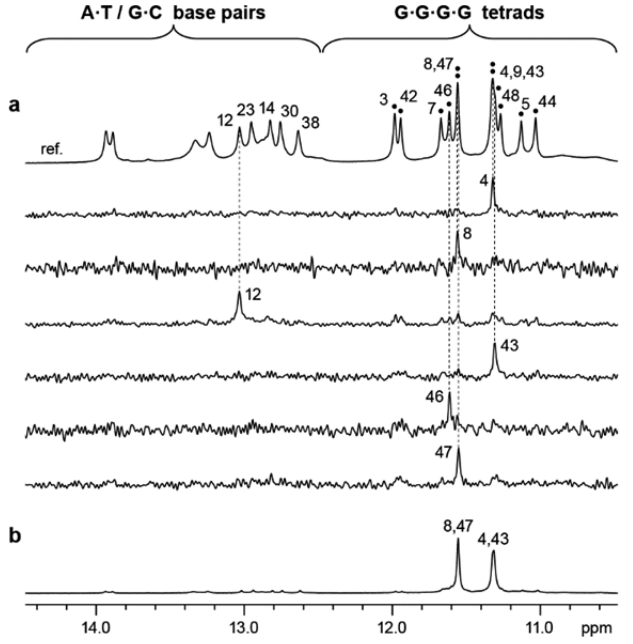

Figure 2. Guanine imino proton assignments of two-stem quadruplex–duplex hybrid construct *2S-QDHL2* in K^+ solution. (a) Examples of imino proton assignments in ^{15}N-filtered spectra of samples, 2–4% ^{15}N-labeled at the indicated positions. The reference spectrum is shown at the top. Imino proton peaks of G-tetrads are indicated with filled circles. Regions corresponding to imino protons taking part in G-tetrad and Watson–Crick base pair formation are demarcated. (b) One-dimensional imino proton NMR spectrum after 1 h in D_2O at 25 °C.

duplex imino proton peaks closely resembled those of the individual duplex stem components (Table S1 and Figure S1, Supporting Information), suggesting successful establishment of the two duplex stems. The structures of the two individual duplex stems, which are closed off by a three-nucleotide hairpin loop (GCA and GAA, respectively), were validated by two-dimensional NMR experiments[8] (data not shown). Chemical shift patterns of the quadruplex imino proton peaks were similar to those of single-stem quadruplex–duplex hybrid constructs (Table S1 and Figure S1, Supporting Information) reported previously,[8,13] in agreement with its adoption of the desired G-tetrad core topology (see validation below). This was also supported by the circular dichroism (CD) spectrum of *2S-QDHL2* (Figure S2, Supporting Information), which was similar to those of single-stem quadruplex–duplex hybrid constructs.[13] The intramolecular folding nature of *2S-QDHL2* was investigated by analysis of the CD-melting profiles across different DNA strand concentrations (see below).

NMR Validation of *2S-QDHL2* Folding Topology. We proceeded to validate the quadruplex–duplex hybrid topology of *2S-QDHL2*. Guanine imino protons were unambiguously assigned through ^{15}N-labeling (2–4%) at individual positions,[28] one residue at a time (Figure 2a; Table S2, Supporting Information). Solvent exchange experiment indicated a slower rate of exchange for the imino protons of G4, G8, G43, and G47 as compared to that for the rest (Figure 2b), in accordance with their central placement in the G-tetrad core. A previously reported site-specific deuteration strategy[29] was adopted in order to define the alignments of the G-tetrad layers for *2S-QDHL2*. Specifically, site-specific ^{2}H-labeling[30] at selective guanine H8 protons of G-tetrads would lead to the disappearance of the corresponding imino-H8 NOE cross-peaks (Figure 3a,b) with the neighboring guanine residues in the G-tetrad (Figure 3c–f), hence establishing the hydrogen-bond directionality of the respective tetrad. Using this approach, the G-tetrad core topology of *2S-QDHL2* was verified to correspond to the expected all-parallel-stranded arrangement (Figure 3g), with the three G-tetrads (G3·G7·G42·G46, G4·G8·G43·G47, and G5·G9·G44·G48) all aligned in the same hydrogen-bond directionality.

Three-Stem Quadruplex–Duplex Hybrid Construct *3S-QDHL2*. To probe a possible incorporation of multiple duplex stems across the same loop of the all-parallel-stranded G-quadruplex scaffold (Figure 1b), a three-stem quadruplex–duplex hybrid complex, d[TT **GGG** T **GGG** T (CGCGAA GCA TTCGCG) (ATCTGA GAA TCAGAT) (AGTCGC GTA GCGACT) T **GGG** T **GGG** T] (henceforth denoted *3S-QDHL2*; Table 1), was constructed. In comparison to *2S-QDHL2*, additional Watson–Crick base-paired imino proton peaks were observed in the one-dimensional imino proton NMR spectrum of *3S-QDHL2* at ~12.6–14 ppm (Figure 4a; Figure S3, Supporting Information), supporting the formation

Table 1. DNA Sequences of Quadruplex–Duplex Hybrids Used in This Study

Name	Sequence[a,b]
2S-QDHL1	TT **GGG** T(CGCGAA GCA TTCGCG)(ATCTGA GAA TCAGAT)T **GGG** T **GGG** T **GGG** T
2S-QDHL2	TT **GGG** T **GGG** T(CGCGAA GCA TTCGCG)(ATCTGA GAA TCAGAT)T **GGG** T **GGG** T
2S-QDHL3	TT **GGG** T **GGG** T **GGG** T(CGCGAA GCA TTCGCG)(ATCTGA GAA TCAGAT)T **GGG** T
3S-QDHL1	TT **GGG** T(CGCGAA GCA TTCGCG)(ATCTGA GAA TCAGAT)(AGTCGC GTA GCGACT)T **GGG** T **GGG** T **GGG** T
3S-QDHL2	TT **GGG** T **GGG** T(CGCGAA GCA TTCGCG)(ATCTGA GAA TCAGAT)(AGTCGC GTA GCGACT)T **GGG** T **GGG** T
3S-QDHL3	TT **GGG** T **GGG** T **GGG** T(CGCGAA GCA TTCGCG)(ATCTGA GAA TCAGAT)(AGTCGC GTA GCGACT)T **GGG** T

[a]G-tracts are shown in bold. [b]Individual duplex stems are enclosed by parentheses, with complementary tracts underlined.

dx.doi.org/10.1021/ja5078816 | J. Am. Chem. Soc. 2014, 136, 17969–17973

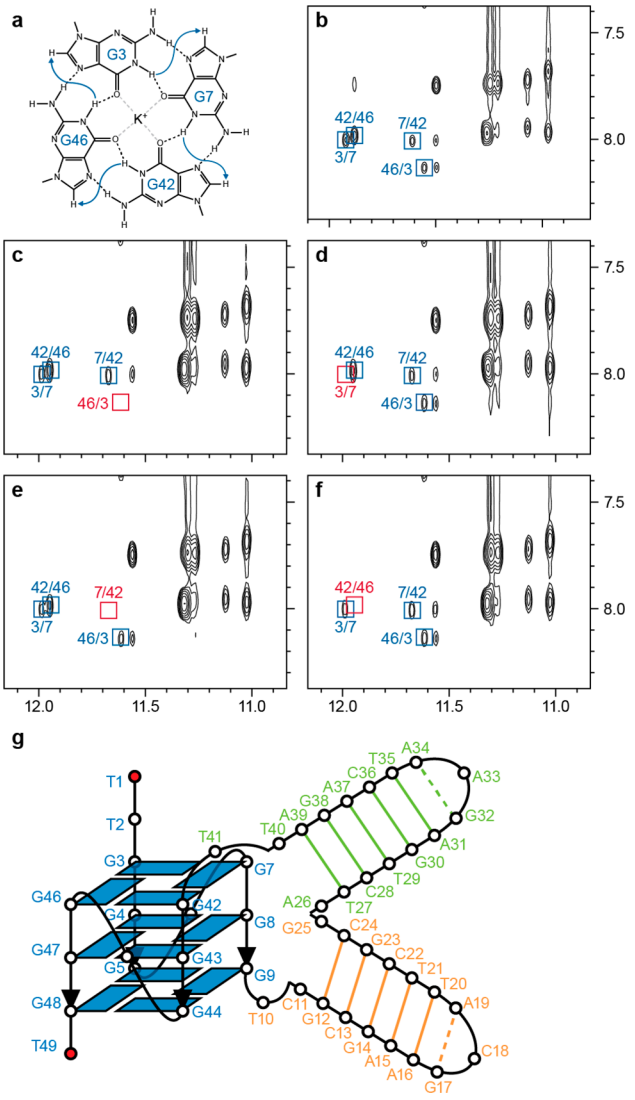

Figure 3. Determination of G-quadruplex folding topology of two-stem quadruplex–duplex hybrid construct *2S-QDHL2* in K^+ solution by site-specific ^2H labeling.[29] (a) Cyclic imino-H8 NOE connectivity patterns within the top G-tetrad layer (G3·G7·G42·G46), as indicated with arrows. (b) NOESY spectrum (mixing time, 200 ms) showing the imino-H8 NOE connectivity patterns of *2S-QDHL2* across the G3·G7·G42·G46 tetrad. Cross-peaks corresponding to the cyclic connectivity patterns are framed and labeled (in blue) with the residue number of imino protons in the first position and that of H8 protons in the second position. Site-specific ^1H-to-^2H substitutions at the H8 position of (c) G3, (d) G7, (e) G42, and (f) G46 led to the disappearance of the corresponding imino-H8 cross-peaks (boxed in red), establishing the hydrogen-bond directionality of the G-tetrad. DNA strand concentration of NMR samples was ~1 mM. (g) Schematic structure of the quadruplex–duplex hybrid adopted by *2S-QDHL2*. Guanine bases of G-tetrads are colored in blue. The two duplex stems are colored separately in orange and green. Watson–Crick and non-canonical base pairs of the duplex stems are represented as solid and dotted lines, respectively. 5′- and 3′-terminal residues are shown as red circles.

of three duplex stems. Furthermore, *3S-QDHL2* displayed highly similar G-tetrad imino proton peak patterns as those of *2S-QDHL2* at ~11–12 ppm (Figure 4a, labeled with filled circles), suggesting a successful adoption of the desired G-tetrad core topology. Establishment of the three duplex stems was corroborated by double guanine/thymine ^{15}N-labeling (2–

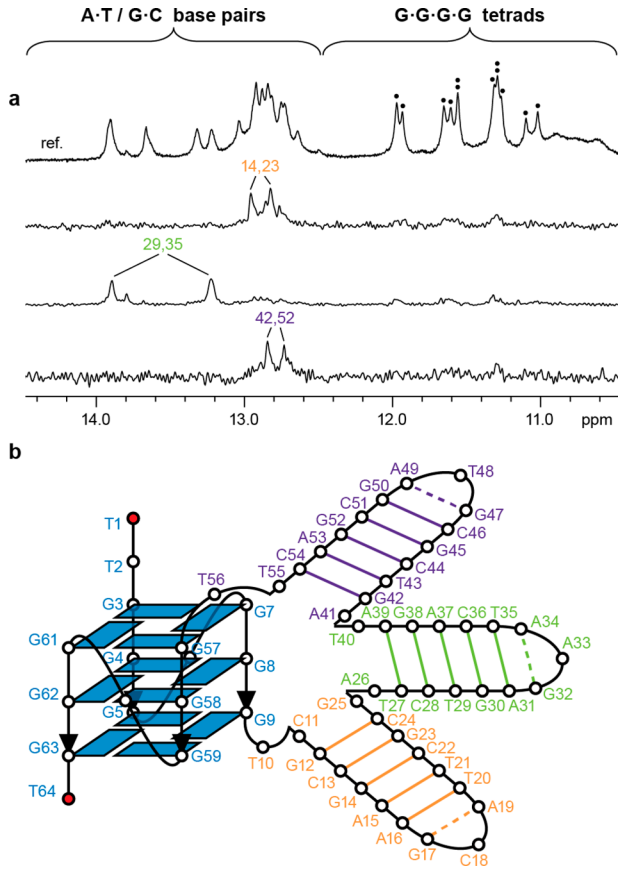

Figure 4. Folding topology of three-stem quadruplex–duplex hybrid construct *3S-QDHL2* in K^+ solution. (a) One-dimensional imino proton NMR spectrum of *3S-QDHL2* in K^+ solution. ^{15}N-filtered spectra of samples, 2–4% ^{15}N-labeled at the indicated positions within the same duplex stems, are shown below. Imino proton peaks of G-tetrads are indicated with filled circles. (b) Schematic structure of the quadruplex–duplex hybrid adopted by *3S-QDHL2*. Guanine bases of G-tetrads are colored in blue. The three duplex stems are colored separately in orange, green, and purple. Watson–Crick and non-canonical base pairs of the duplex stems are represented as solid and dotted lines, respectively. 5′- and 3′-terminal residues are shown as red circles.

4%) within each stem (Figure 4a; Table S3, Supporting Information). The CD spectrum of *3S-QDHL2* (Figure S2, Supporting Information) was also similar to those of single-stem quadruplex–duplex hybrid constructs reported previously.[13]

Thermal Stability of *2S-QDHL2* and *3S-QDHL2*. Thermal stability of *2S-QDHL2* in the presence of ~50 mM K^+ was measured by the CD signal transition at 262 nm,[13] giving a melting temperature (T_m) of ~(56 ± 2) °C across different DNA strand concentrations (2 μM, 54.3 °C; 4 μM, 54.3 °C; 50 μM, 57.4 °C; 100 μM, 58.4 °C; Figure S4, Supporting Information). Small changes in T_m were observed for strand concentrations from 2 to 100 μM, consistent with the intramolecular nature of the major conformation. The T_m value of *3S-QDHL2*, on the other hand, was found to be ~47 °C.

Here, our measurement based on the CD signal transition at 262 nm provides an estimate on the melting process of the quadruplex segment alone.[13] Interplay between the duplex and quadruplex components are important considerations for the implementation of multi-stem quadruplex–duplex hybrid

dx.doi.org/10.1021/ja5078816 | J. Am. Chem. Soc. 2014, 136, 17969–17973

motifs in DNA nanotechnology, as well as their potential formation in a biological context. The presence of duplex stems within the loop of the quadruplex led to a positive influence on the stability of the quadruplex, relative to that of a non-structured loop of similar lengths (T_m of *2S-QDHL2*, a quadruplex containing two duplex stems within a 32-nt loop, was ~54 °C, compared to ~50 and ~48 °C for equivalent quadruplexes containing a non-structured loop of T_{27} and T_{37}, respectively).[13] However, melting transitions of the duplex and quadruplex components do not necessarily occur simultaneously; T_m of the quadruplex was lower than that of the duplexes under low K^+, high Li^+ conditions (data not shown), whereas the reverse should apply for weak duplexes (e.g., comprising mismatched base pairs) under high K^+ conditions.

Structural Contexts at the Quadruplex–Duplex Junction. The context at the junction between the quadruplex and duplex components is highly influential toward the stability and structural integrity of quadruplex–duplex hybrid complexes.[13] In the case of the two- and three-stem constructs examined here, guanine/thymine imino proton peaks were not observed for the potential immediate base pairs at the junction (C11·G25 and A26·T40 for *2S-QDHL2*; C11·G25, A26·T40, and A41·T55 for *3S-QDHL2*), suggesting that their formation might have been disrupted. On the other hand, the next base pairs down the stem are more stably established, supported by sharp imino proton peaks of G12 (for *2S-QDHL2*) and G42 (for *3S-QDHL2*).

In previous instances of single-stem quadruplex–duplex hybrids, the base pair at the junction was found to be extruded.[8] It was also shown that these bulged nucleotides bridging the quadruplex–duplex junction can be extended up to three nucleotides without adversely affecting the stability of quadruplex–duplex hybrids for which the duplex stem projects out as a propeller loop.[13] Similar behavior could be expected of the multi-stem constructs examined here because the duplex stems are also projected out of the tetrad core in a sideway manner. We note that the size of these two bulges at the junction would affect global orientation of the various duplex stems within the loop.

Diverse Structures of Multi-Stem Quadruplex–Duplex Hybrid Complexes. We have shown that quadruplex–duplex hybrid complexes harboring two (*2S-QDHL2*) and three (*3S-QDHL2*) duplex stems within the same loop of a quadruplex can exist. In both constructs, the duplex stems were incorporated within the middle propeller loop of an all-parallel-stranded G-tetrad core.[26,27] Incorporation of these duplex stems in the first (i.e., *2S-QDHL1* and *3S-QDHL1*; Table 1) or third (i.e., *2S-QDHL3* and *3S-QDHL3*; Table 1) propeller loop of the same quadruplex construct also led to the establishment of the expected quadruplex–duplex hybrid structures (Figure S5, Supporting Information). We note that this multi-stem incorporation strategy could also be applicable to other G-tetrad core topologies (e.g., antiparallel-stranded basket-type or (3 + 1) G-quadruplex scaffold) and/or different loop configurations (i.e., edgewise or diagonal loop).

In a structural context, the two-stem construct *2S-QDHL2* can be regarded as a variation of the three-way junction, whereas the three-stem construct *3S-QDHL2*, a variation of the four-way junction, wherein the quadruplex unit takes over the place of one duplex arm in each case. In principle, incorporation of four or more duplex stems within the same quadruplex loop could also be possible. Previously, 8- and 12-arm branched DNA junctions were successfully constructed.[31] It would be interesting to find out if any number of these stems can be substituted with quadruplex units.

Biological Relevance of Multi-Stem Quadruplex–Duplex Hybrids. The joining of multiple duplex stems at a single quadruplex loop brings forward a myriad of possibilities in which a quadruplex structure (either intramolecular or intermolecular in nature) can arise, wherein complementary bases of the duplex stems facilitate the congregation of G-tracts. We have identified sequence motifs capable of forming intramolecular single-stem quadruplex–duplex hybrids in the human genome (unpublished data). The potential existence of more complex sequence motifs in the human genome could reveal as yet unknown biological functions and would give rise to exciting opportunities for therapeutic targeting because the interface between quadruplex and duplex segments could provide unique structural features for specific ligand binding.

■ CONCLUSIONS

We showed here the simultaneous incorporation of two and three duplex stems within the same loop of a quadruplex to generate stable quadruplex–duplex hybrid structures. The multi-stem quadruplex–duplex hybrid complexes presented offer new design principles for the construction of DNA architectures, in which the G-tetrad core serves as a robust scaffold for the coordination of multiple duplex stems. In addition, the potential existence of such complex motifs in genomic sequences could have biological implications and would represent unique targets for the design of chemical ligands.

■ METHODS

DNA Sample Preparation. DNA oligonucleotides were chemically synthesized on an ABI 394 DNA/RNA synthesizer. The oligonucleotides were deprotected with aqueous ammonium hydroxide and purified using Poly-Pak cartridges. Samples were dialyzed successively against water, 20 mM KCl solution, and water again.

NMR Spectroscopy. Lyophilized DNA samples were suspended in a buffer containing 20 mM KCl and 20 mM potassium phosphate (pH 7.0), with a typical strand concentration of 0.2–2.0 mM. One- and two-dimensional NMR spectra were recorded on Bruker AVANCE 600- and 700-MHz spectrometers at 25 °C, unless otherwise specified. Unambiguous assignments of the proton resonances for guanine and thymine residues were determined from site-specific low-enrichment ^{15}N-labeling[28] and site-specific ^{2}H-labeling.[30]

Circular Dichroism. CD spectra were recorded over the range of 220–320 nm on a Jasco-815 spectropolarimeter. Each spectrum is obtained as an average of three scans, with the spectrum of the buffer subtracted. Cooling and heating experiments were performed across the temperature range of 15–95 °C as described previously.[13] Signal transition at 262 nm was used for the characterization of the melting process of the quadruplex–duplex hybrids. The buffer contained 20 mM KCl and 20 mM potassium phosphate (pH 7.0). Unless otherwise specified, concentrations of DNA samples were 4 μM.

■ ASSOCIATED CONTENT

Ⓢ Supporting Information

Table S1: Sequences of reference quadruplex and duplex stems (*1S-QDHL2, dx1, dx2, and dx3*) used in this study. Table S2: Site-specific labeled DNA sequences of *2S-QDHL2* used in this study. Table S3: Site-specific labeled DNA sequences of *3S-QDHL2* used in this study. Figure S1: One-dimensional imino proton NMR spectra of *2S-QDHL2*, *1S-QDHL2*, *dx1*, and *dx2*. Figure S2: CD spectra of *2S-QDHL2* and *3S-QDHL2* at 25 °C. Figure S3: One-dimensional imino proton NMR spectra of *3S-QDHL2*, *1S-QDHL2*, *dx1*, *dx2*, and *dx3*. Figure S4: Fractions of

dx.doi.org/10.1021/ja5078816 | J. Am. Chem. Soc. 2014, 136, 17969–17973

folded G-quadruplexes as a function of temperature at different DNA strand concentrations of *2S-QDHL2*. Figure S5: One-dimensional imino proton NMR spectra of *2S-QDHL1*, *2S-QDHL3*, *3S-QDHL1*, and *3S-QDHL3*. This material is available free of charge via the Internet at http://pubs.acs.org.

AUTHOR INFORMATION

Corresponding Author

phantuan@ntu.edu.sg

Author Contributions

[†]K.W.L. and T.Q.N.N. contributed equally to this work.

Notes

The authors declare no competing financial interest.

ACKNOWLEDGMENTS

This research was supported by Singapore Ministry of Education Academic Research Fund Tier 3 (MOE2012-T3-1-001) and Tier 2 (MOE2012-T2-1-102) and grants from Nanyang Technological University to A.T.P.

REFERENCES

(1) Lilley, D. M. J. *Q. Rev. Biophys.* **2000**, *33*, 109−159.
(2) Holliday, R. *Genet. Res.* **1964**, *5*, 282−304.
(3) Szostak, J. W.; Orr-Weaver, T. L.; Rothstein, R. J.; Stahl, F. W. *Cell* **1983**, *33*, 25−35.
(4) Jaeger, L.; Chworos, A. *Curr. Opin. Struct. Biol.* **2006**, *16*, 531−543.
(5) Eichman, B. F.; Vargason, J. M.; Mooers, B. H. M.; Ho, P. S. *Proc. Natl. Acad. Sci. U.S.A.* **2000**, *97*, 3971−3976.
(6) Seeman, N. C. *Annu. Rev. Biochem.* **2010**, *79*, 65−87.
(7) Ha, S. C.; Lowenhaupt, K.; Rich, A.; Kim, Y. G.; Kim, K. K. *Nature* **2005**, *437*, 1183−1186.
(8) Lim, K. W.; Phan, A. T. *Angew. Chem., Int. Ed.* **2013**, *52*, 8566−8569.
(9) Burge, S.; Parkinson, G. N.; Hazel, P.; Todd, A. K.; Neidle, S. *Nucleic Acids Res.* **2006**, *34*, 5402−5415.
(10) Patel, D. J.; Phan, A. T.; Kuryavyi, V. *Nucleic Acids Res.* **2007**, *35*, 7429−7455.
(11) Gellert, M.; Lipsett, M. N.; Davies, D. R. *Proc. Natl. Acad. Sci. U.S.A.* **1962**, *48*, 2013−2018.
(12) Yu, Z. B.; Gaerig, V.; Cui, Y. X.; Kang, H. J.; Gokhale, V.; Zhao, Y.; Hurley, L. H.; Mao, H. B. *J. Am. Chem. Soc.* **2012**, *134*, 5157−5164.
(13) Lim, K. W.; Khong, Z. J.; Phan, A. T. *Biochemistry* **2014**, *53*, 247−257.
(14) Ge, B. X.; Huang, Y. C.; Sen, D.; Yu, H. Z. *Angew. Chem., Int. Ed.* **2010**, *49*, 9965−9967.
(15) Dutta, K.; Fujimoto, T.; Inoue, M.; Miyoshi, D.; Sugimoto, N. *Chem. Commun.* **2010**, *46*, 7772−7774.
(16) Yatsunyk, L. A.; Mendoza, O.; Mergny, J. L. *Acc. Chem. Res.* **2014**, *47*, 1836−1844.
(17) Todd, A. K.; Johnston, M.; Neidle, S. *Nucleic Acids Res.* **2005**, *33*, 2901−2907.
(18) Huppert, J. L.; Balasubramanian, S. *Nucleic Acids Res.* **2005**, *33*, 2908−2916.
(19) Maizels, N.; Gray, L. T. *PLoS Genet.* **2013**, *9*, e1003468.
(20) Huppert, J. L.; Balasubramanian, S. *Nucleic Acids Res.* **2007**, *35*, 406−413.
(21) Eddy, J.; Maizels, N. *Nucleic Acids Res.* **2008**, *36*, 1321−1333.
(22) Huppert, J. L.; Bugaut, A.; Kumari, S.; Balasubramanian, S. *Nucleic Acids Res.* **2008**, *36*, 6260−6268.
(23) Hazel, P.; Huppert, J.; Balasubramanian, S.; Neidle, S. *J. Am. Chem. Soc.* **2004**, *126*, 16405−16415.
(24) Rachwal, P. A.; Findlow, I. S.; Werner, J. M.; Brown, T.; Fox, K. R. *Nucleic Acids Res.* **2007**, *35*, 4214−4222.
(25) Guédin, A.; Gros, J.; Alberti, P.; Mergny, J. L. *Nucleic Acids Res.* **2010**, *38*, 7858−7868.
(26) Trajkovski, M.; da Silva, M. W.; Plavec, J. *J. Am. Chem. Soc.* **2012**, *134*, 4132−4141.
(27) Do, N. Q.; Phan, A. T. *Chem.—Eur. J.* **2012**, *18*, 14752−14759.
(28) Phan, A. T.; Patel, D. J. *J. Am. Chem. Soc.* **2002**, *124*, 1160−1161.
(29) Yue, D. J. E.; Lim, K. W.; Phan, A. T. *J. Am. Chem. Soc.* **2011**, *133*, 11462−11465.
(30) Huang, X. N.; Yu, P. L.; LeProust, E.; Gao, X. L. *Nucleic Acids Res.* **1997**, *25*, 4758−4763.
(31) Wang, X.; Seeman, N. C. *J. Am. Chem. Soc.* **2007**, *129*, 8169−8176.